

Conformational States of the Severe Acute Respiratory Syndrome Coronavirus Spike Protein Ectodomain

Fang Li,¹ Marcelo Berardi,² Wenhui Li,³ Michael Farzan,³
Philip R. Dormitzer,¹ and Stephen C. Harrison^{1,2,4*}

Laboratory of Molecular Medicine, Children's Hospital,¹ and Howard Hughes Medical Institute,⁴ Boston, Massachusetts 02115;
Department of Biological Chemistry and Molecular Pharmacology, Harvard Medical School, Boston, Massachusetts 02115²;
and Department of Microbiology and Molecular Genetics, Harvard Medical School, and New England Primate Center,
Southborough, Massachusetts 01772³

Received 30 December 2005/Accepted 3 May 2006

The severe acute respiratory syndrome coronavirus enters cells through the activities of a spike protein (S) which has receptor-binding (S1) and membrane fusion (S2) regions. We have characterized four sequential states of a purified recombinant S ectodomain (S-e) comprising S1 and the ectodomain of S2. They are S-e monomers, uncleaved S-e trimers, cleaved S-e trimers, and dissociated S1 monomers and S2 trimer rosettes. Lowered pH induces an irreversible transition from flexible, L-shaped S-e monomers to clove-shaped trimers. Protease cleavage of the trimer occurs at the S1-S2 boundary; an ensuing S1 dissociation leads to a major rearrangement of the trimeric S2 and to formation of rosettes likely to represent clusters of elongated, postfusion trimers of S2 associated through their fusion peptides. The states and transitions of S suggest conformational changes that mediate viral entry into cells.

The severe acute respiratory syndrome (SARS) coronavirus (CoV) is the agent of the SARS epidemics in 2002 to 2003 and 2003 to 2004 (11, 18). The spike protein, S, forms prominent projections from the SARS CoV envelope. It directs cell entry by binding to its receptor, angiotensin-converting enzyme 2 (ACE2), on the cell surface (15) and by fusing the viral and host membranes (3). Previous biochemical studies on the S protein from murine hepatitis virus (MHV), the best-studied member of the *Coronavirus* family, show that it has a large ectodomain (about 1,200 residues), a transmembrane region, and a short intracellular tail (13). During export to the cell surface, MHV S is cleaved by a cellular protease into two fragments, a receptor-binding fragment (S1) and a fusogen (S2) (25). The SARS CoV S protein is not cleaved prior to virion assembly, but sequence alignment with MHV S (and other coronavirus S proteins) allows unambiguous definition of S1 and S2 regions (16, 19). The S2 region, like the S2 fragment of MHV S, contains two heptad repeat segments, HR1 and HR2, which form coiled coils in vitro (2, 30, 31). Coiled-coil formation is central to the mechanism of class I fusion proteins, which include envelope glycoproteins from influenza virus, human immunodeficiency virus, Ebola virus, and measles virus (23).

A class I viral fusion protein is expressed as a single-chain precursor. During maturation, the precursor trimerizes and cellular proteases cleave the chains into receptor-binding and membrane fusion fragments (10, 27). The metastable, cleaved form can be triggered to rearrange; the ensuing conformational transitions catalyze fusion (8, 23). In the first phase of this transition, a fusion peptide unfolds, projects toward the

target cell surface, and inserts into the cellular membrane. During the second phase, the fragment refolds into a trimer of hairpins in which the first heptad region forms a central, three-stranded coiled coil and the second heptad repeat forms an outer layer. The fusion peptide, inserted in the cell membrane, and the transmembrane anchor, which traverses the viral envelope, are thus brought together, drawing the two membranes together as well. Depending on the virus, the rearrangement may be triggered by receptor binding, a change in pH, or a combination of the two; it may occur at the cell surface or in the endosome (23). In the case of SARS CoV, cleavage by cathepsin L, following viral uptake into endosomes, appears to be required for entry (20).

The S1 region of the SARS CoV S protein contains a discrete domain that interacts with ACE2 (1, 28, 29). The structure of this domain bound with a truncated ACE2 ectodomain has illustrated in atomic detail the molecular interactions that determine initial viral attachment (14). How does this view of one step in the entry process relate to the molecular organization of the intact S protein? We show here that the purified, recombinant, SARS CoV S protein ectodomain undergoes a series of conformational transitions, which resemble those of other enveloped virus fusion proteins but with some specific features probably relevant to the pathway of viral entry.

MATERIALS AND METHODS

Protein expression and purification. The full-length ectodomain (residues 12 to 1190) of the SARS CoV S protein (S-e) fused to an N-terminal honeybee melittin signal sequence and a C-terminal histidine tag was expressed in Sf9 insect cells. The vector was constructed with the Bac-to-Bac expression system (Life Technologies Inc.). Insect cell supernatants were harvested 4 days after recombinant baculovirus infection and concentrated by ultrafiltration (Millipore). S-e in the concentrated supernatant was purified to homogeneity by lectin affinity chromatography on concanavalin A Sepharose (Amersham Biosciences) with elution by 0.5 M mannose, followed by metal affinity chromatography on Ni-nitrilotriacetic acid resin (Amersham Biosciences) with elution by 0.5 M

* Corresponding author. Mailing address: HHMI/Children's Hospital, Laboratory of Molecular Medicine, 320 Longwood Ave., Boston, MA 02115. Phone: (617) 355-7372. Fax: (617) 730-1967. E-mail: harrison@crystal.harvard.edu.

imidazole, followed by gel filtration chromatography on Superdex 200 (Amersham Biosciences) in buffer A (10 mM Tris [pH 7.2], 100 mM NaCl).

Preparation of S-e trimer. Purified S-e monomer in buffer A was exposed to a low pH by adding 1/10 volume of 1 M sodium citrate (pH 5.6). After 1 h of incubation at room temperature, trimeric S-e was isolated by gel filtration chromatography on Superdex 200 at 4°C in buffer A. Fractions corresponding to the S-e trimer were identified by the elution volume of the main peak of absorption (280 nm) and concentrated by ultrafiltration.

Proteolysis. S-e trimer (1 mg/ml in buffer A) was incubated with 5 µg/ml TPCK (L-1-tosylamide-2-phenylmethyl chloromethyl ketone)-treated trypsin (Worthington Biochemical) for 30 min at room temperature. Digestion was stopped by adding phenylmethylsulfonyl fluoride (PMSF) to 1 mM. The cleaved trimer was separated from trypsin, and the buffer was exchanged by gel filtration chromatography with Superdex 200 in buffer A.

To map trypsin cleavage sites, purified S-e (0.2 mg/ml in buffer A) was incubated with 1 µg/ml TPCK-treated trypsin for 30 min at room temperature. Digestion was stopped by adding PMSF to 1 mM. Digestion products were separated by sodium dodecyl sulfate-polyacrylamide gel electrophoresis (SDS-PAGE), electroblotted onto a Sequiblot polyvinylidene difluoride (PVDF) membrane (Bio-Rad), stained with Coomassie blue, excised, and identified by N-terminal sequencing at the Tufts Protein Chemistry Facility (Boston, MA).

Preparation of S2 rosettes. To accelerate rosette formation, 1/5 volume of 5 M urea was added to cleaved S-e trimer in buffer A. The sample was incubated for 2 h at room temperature before analysis by electron microscopy or repurification. Rosettes, whether formed spontaneously from S-e trimers stored at 4°C or induced by urea treatment, were isolated in the void volume after gel filtration chromatography on Superdex 200 in buffer A.

Chemical cross-linking. Purified S-e, 0.2 mM in phosphate-buffered saline, was incubated with 0.01 to 5 mM ethylene glycol-bis(succinimidylsuccinate) (EGS; Pierce). After 30 min of incubation at room temperature, the reactions were quenched by adding 1/10 volume of 1 M Tris-Cl, pH 8.1.

Analytical ultracentrifugation. Protein samples were analyzed in a Beckman XL-A analytical ultracentrifuge with an AN-60 Ti rotor at 4°C at concentrations of 0.25, 0.50, and 0.75 mg/ml in buffer A. The S-e monomer was centrifuged to equilibrium at 10,500 rpm and 13,500 rpm; the S-e trimer was centrifuged to equilibrium at 5,500 rpm. The protein concentration distributions, as measured by A_{280} with three replicates, were fitted to a single-species model with the formula $A_r = A_{0,1} \exp[HM(x^2 - x_0^2)] + E$, where A_r is the absorbance at radius x ; $A_{0,1}$ is the absorbance at the reference radius x_0 ; H is a constant to account for the specific volume of the protein, the solvent density, the angular velocity of the rotor, and the temperature; M is the monomer molecular weight; and E is the baseline offset. $A_{0,1}$ is constrained to be greater than 0. Protein partial specific volume (0.71 ml/g) and solvent density (1.01 g/ml) were calculated from amino acid composition.

Mass spectrometry. Matrix-assisted laser desorption ionization–time of flight mass spectrometry of the S-e monomer was performed at the Tufts Protein Chemistry Facility (Boston, MA). Mass spectrometry of the EGS-cross-linked S-e trimer was carried out at the Howard Hughes Medical Institute Mass Spectrometry Laboratory at University of California (Berkeley, CA).

Electron microscopy. Protein samples were diluted to 10 to 100 µg/ml by dilution with water, adsorbed to glow-discharged carbon grids for 2 min, washed with deionized water, and negatively stained with freshly prepared 0.75% uranyl formate. Images were obtained at magnifications of $\times 15,000$ to $\times 39,000$ with a CM10 electron microscope (Philips) operated at 100 kV.

RESULTS

We expressed the S-e of SARS CoV in Sf9 cells as a secreted, C-terminally histidine-tagged protein and purified it by affinity and gel filtration chromatography (Fig. 1A, lane a, and B, trace a). Its molecular mass, 157 kDa as determined by mass spectrometry (not shown), is in excellent agreement with the mass calculated from its amino acid sequence, assuming that each of the 23 potential N-glycosylation sites bears a 1-kDa oligosaccharide (the most common, mannose-rich structure found on insect cell expressed proteins). Equilibrium analytical ultracentrifugation shows that at neutral pH, S-e is a homogeneous monomer (Fig. 1C). Gel filtration chromatography of S-e yields a single homogeneous peak (Fig. 1B, trace a) with a Stokes radius of 43 Å, which corresponds to an axial ratio of

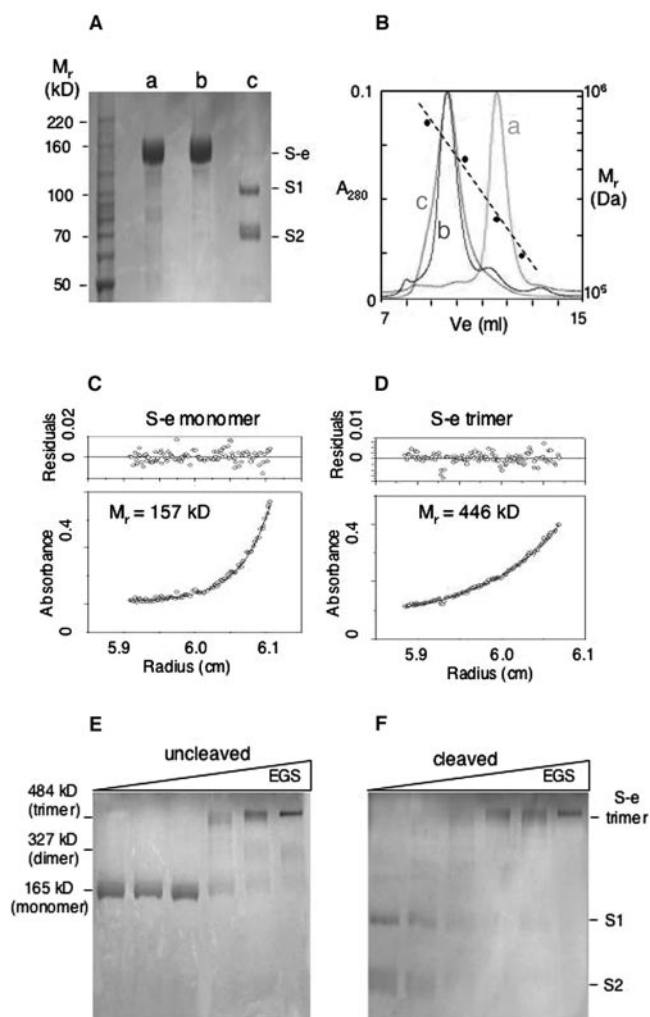


FIG. 1. Oligomeric states of the purified recombinant SARS coronavirus S-e. (A) Coomassie blue-stained reducing SDS-PAGE. Lane a, as purified from insect cell medium; lane b, exposed to pH 5.6; lane c, exposed to pH 5.6 and then digested (at neutral pH) with 200 ng/ml trypsin. (B) Gel filtration chromatography on Superdex 200. Samples correspond to those in panel A, as indicated by the lettering of the chromatograms. Black circles indicate migration of calibration standards (thyroglobulin, 669 kDa; ferritin, 440 kDa; catalase, 232 kDa; aldolase, 158 kDa). The fitted curve is a dotted line. The apparent molecular mass is 226 kDa for the monomer and 520 kDa for both intact and cleaved trimers. (C) Equilibrium analytical ultracentrifugation of purified S-e. Blue circles indicate the concentration distribution (A_{280}) of a 0.25-mg/ml sample at 10,500 rpm. The curve indicates the theoretical distribution of a 157-kDa particle. (D) Analytical ultracentrifugation of S-e after exposure to pH 5.6. Circles show the equilibrium distribution (A_{280}) of a 0.25-mg/ml sample at 5,500 rpm. The curve shows the theoretical distribution of a 446-kDa particle. (E) Chemical cross-linking of S-e after exposure to pH 5.6. Prior to separation by SDS-PAGE and staining with Coomassie blue, low-pH-treated S-e was incubated with (from left to right) 0, 0.01, 0.05, 0.2, 1, or 5 mM EGS. The indicated molecular masses were determined by mass spectrometry. (F) Chemical cross-linking of S-e after exposure to pH 5.6 and cleavage with 200 ng/ml trypsin. Samples were analyzed as in panel E.

2.1 at a hydration of 0.4 g/g for a 157-kDa protein. Negative-stain electron microscopy reveals an elongated molecule, often L shaped as adsorbed to the carbon film, with a contour length of about 160 Å (Fig. 2A).

Treatment of the S-e monomer with low concentrations of

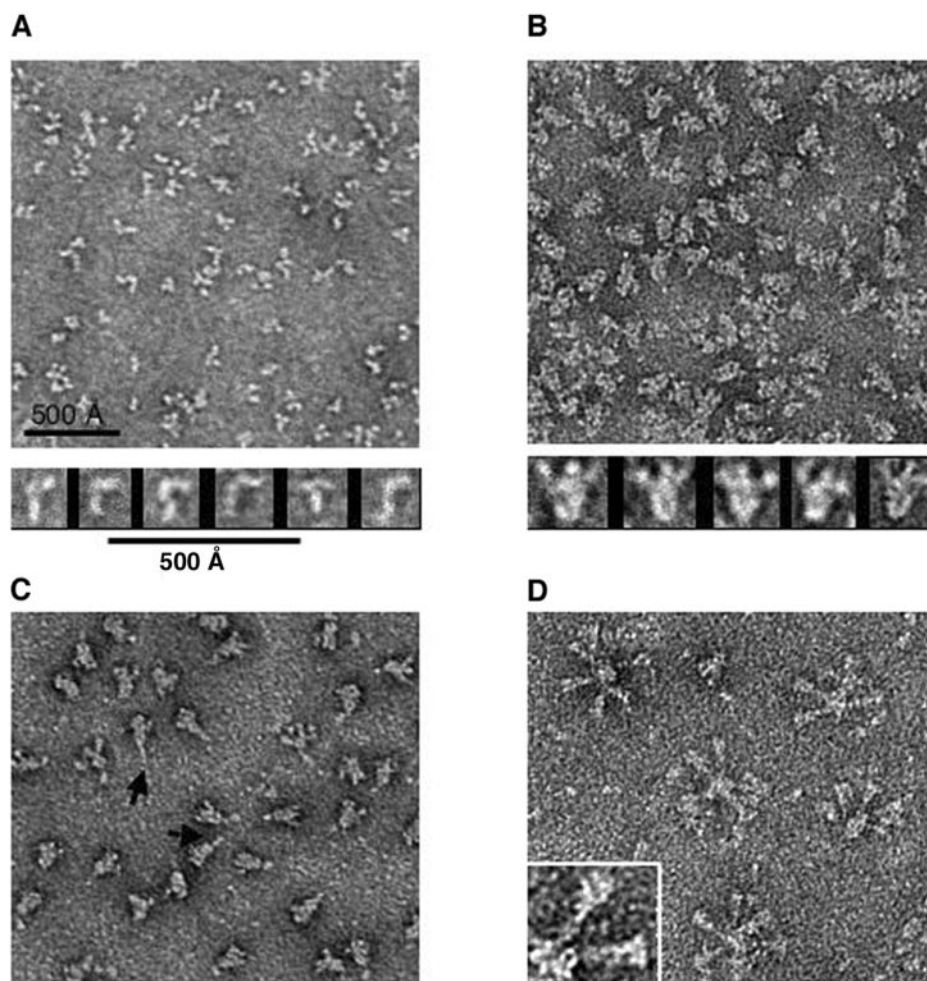


FIG. 2. Electron micrographs of S-e preparations. (A) S-e monomers have an L shape with variable morphology. (B) After exposure to pH 5.6, S-e trimers have a homogeneous clove-like shape with three knobs at the broader end of a tapered shaft. (C) After trypsin cleavage, most S-e trimers retain the morphology seen in panel B. Several molecules show evidence of rearrangement at one end (arrows). (D) After cleaved trimers have been incubated in 1 M urea for 2 h at room temperature, a field of rosettes is obtained. The inset shows part of one rosette. The short and long scale bars in panel A apply to all of the electron microscopy fields and extracted individual images (including the inset in panel D), respectively. All samples were stained with 0.75% uranyl formate.

trypsin yields two fragments with apparent masses of 100 kDa and 70 kDa by SDS-PAGE (Fig. 3A, lane 2). N-terminal sequencing and mass spectrometry show that the larger and smaller fragments correspond to the S1 and S2 regions, respectively. The site of cleavage aligns precisely with the site that separates S1 and S2 in MHV (Fig. 3B). The two fragments dissociate from each other; S1 remains soluble, migrating on gel filtration chromatography with a Stokes radius of 39 Å, while S2 forms an aggregate that can be removed by low-speed centrifugation (Fig. 3C).

Exposure of the S-e monomer to a pH of <6 leads to a shift in its gel filtration elution profile (Fig. 1B, trace b). The apparent molecular mass is 520 kDa, and the Stokes radius is 71 Å. Analytical ultracentrifugation, chemical cross-linking with EGS, and mass spectrometry show that the protein is now a trimer (Fig. 1D and E). The low-pH-induced trimerization is irreversible, as a return to neutral pH does not lead to dissociation, and the trimer appears to be quite stable. Negative-stain electron microscopy of the trimer reveals a clove-shaped

molecule with three knobs at one end of a slightly tapered rod (Fig. 2B). The overall length of the trimer is about 160 Å.

Like the monomer, trimeric S-e is cleaved specifically by trypsin at the S1-S2 boundary, as shown by SDS-PAGE and confirmed by N-terminal sequencing (Fig. 3A, lane 7, and B). Higher concentrations of trypsin lead to further digestion of the S1 fragment, but the S2 fragment is resistant even to a very high level of the protease (1 mg/ml) (Fig. 3A, lane 10). In contrast, trypsin at a high concentration degrades both fragments of the monomer (Fig. 3, lane 5). Thus, trimer formation upon transient exposure to a low pH renders S2 selectively protease insensitive, consistent with the structural rearrangement detected by electron microscopy. Most of the trypsin-cleaved S-e trimers retain the shape of the uncleaved trimer, as shown by electron microscopy (Fig. 2C), and the gel filtration profile is unaltered (Fig. 1B, trace c). At high EGS concentrations, the cleaved trimer can be cross-linked to a species with the same mobility on SDS-PAGE as the cross-linked uncleaved trimer (Fig. 1F). No change in the shape or structure of the

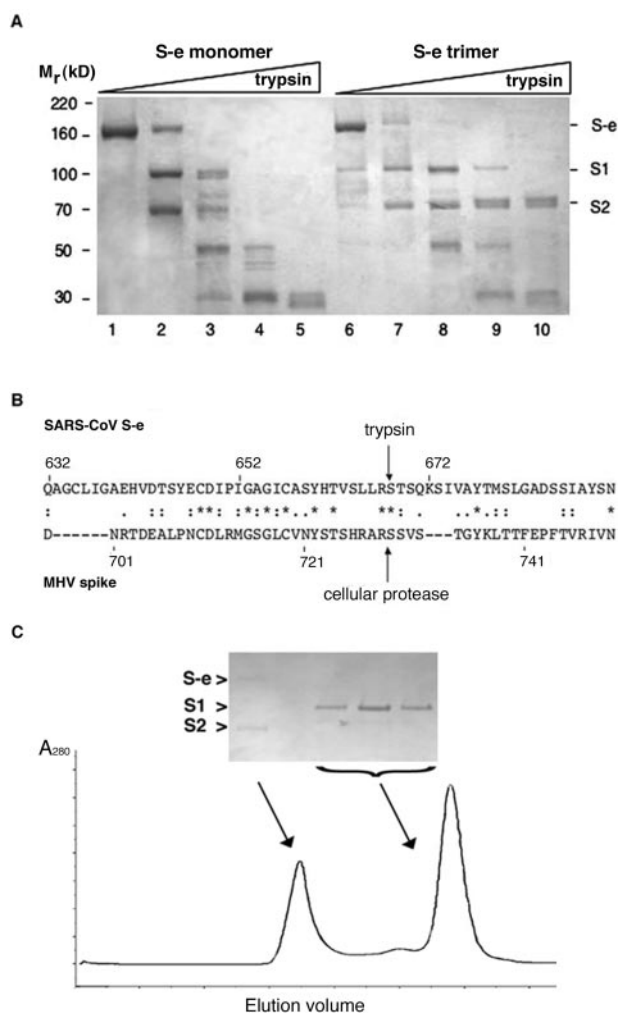


FIG. 3. Trypsin cleavage of S-e. (A) S-e monomers (lanes 1 to 5) and trimers (lanes 6 to 10) were incubated at room temperature for 30 min with trypsin (0, 10^{-4} , 10^{-3} , 10^{-2} , and 1 mg/ml for lanes 1 to 5 and 6 to 10). After quenching with PMSF, the samples were resolved by SDS-PAGE and stained with Coomassie blue. (B) Sequence alignment of the SARS CoV and MHV (strain 2, accession number AF201929) S proteins at the S1-S2 boundary region. The arrows indicate the trypsin cleavage site in the SARS CoV S protein and the site of cleavage by a cellular protease in the MHV S protein. (C) Gel filtration chromatography of the products of tryptic cleavage of S-e monomers. (Inset) SDS-PAGE analysis of the void volume and of the peak. The peak contains soluble, monomeric S-1; the void contains residual aggregated S-2 (some of which precipitates) and a trace of uncleaved S-e.

trimer is observed even after digestion with 1 mg/ml trypsin (not shown).

Soluble ACE2 binds both monomers and trimers of S-e. Electron microscopy of trimers with bound ACE2 shows that the receptor decorates the knobs at the wider end of the clove-shaped assembly (Fig. 4). We conclude that the knobs contain the receptor-binding domain (RBD) and possibly additional parts of S1.

Further conformational rearrangement can occur after protease cleavage of trimeric S-e if S1 is induced to dissociate. Images of negatively stained, cleaved trimers contain some

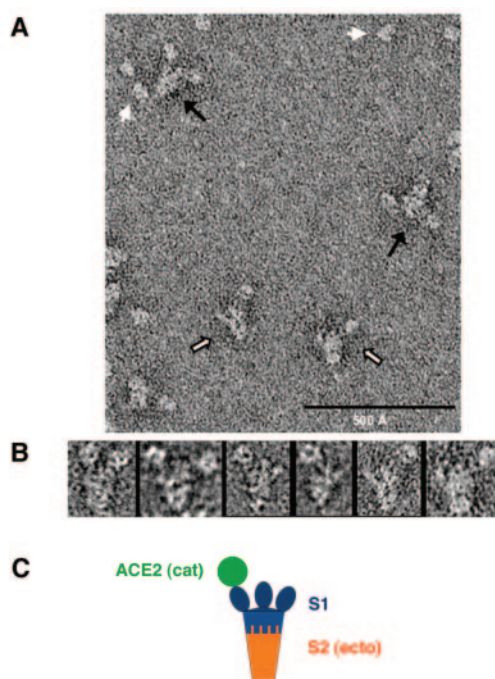


FIG. 4. Binding of the soluble ACE2 catalytic domain to uncleaved trimeric S-e. (A) Field of complexes negatively stained with uranyl formate. The molar ratio of the ACE2 catalytic domain to the S-e trimer was 10:1. Black arrows, trimers with at least two bound ACE2 catalytic domains; hollow black arrows, trimers with a single bound ACE2; white arrows, free ACE2 catalytic domain. (B) Gallery of images from panel A and other, similar fields. (C) Interpretative diagram. The ACE2 catalytic domain [ACE2(cat)] associates with the bumps on the trimer, schematized here as ovals, which therefore contain the RBD and perhaps additional parts of the S polypeptide chain (14).

clove-shaped particles that appear to have a tail at the narrow end, as if the protein is starting to rearrange (Fig. 2C, arrow). Occasional rosette-like structures, not seen in preparations of the uncleaved trimer, also appear. Incubation of cleaved S-e trimers in 1 M urea at room temperature causes most of the protein to form rosettes (Fig. 2D). The rosettes contain 3 to 10 rods, each about 250 Å in length, radiating from a common point. Each rod has a dumbbell shape, with globular structures at both ends and a thin bar in the middle (Fig. 2D, inset). Upon gel filtration, these spontaneously formed rosettes are enriched in the void volume (Fig. 5A and C). SDS-PAGE shows that they contain only S2 (Fig. 5B). Urea treatment of S-e monomers or uncleaved S-e trimers does not lead to rosette formation (not shown).

DISCUSSION

The biochemical properties and conformational states of the purified ectodomains of viral fusion proteins reflect the way these proteins carry out viral entry (23). We have identified four distinct sequential forms of the SARS coronavirus S-e and in vitro conditions that produce irreversible transitions from one form to the next (summarized in Fig. 6). These forms are S-e monomers, uncleaved S-e trimers, cleaved S-e trimers, and a dissociated state with soluble S1 monomers and rosette-forming, extended S2 trimers. Exposure to low pH triggers the

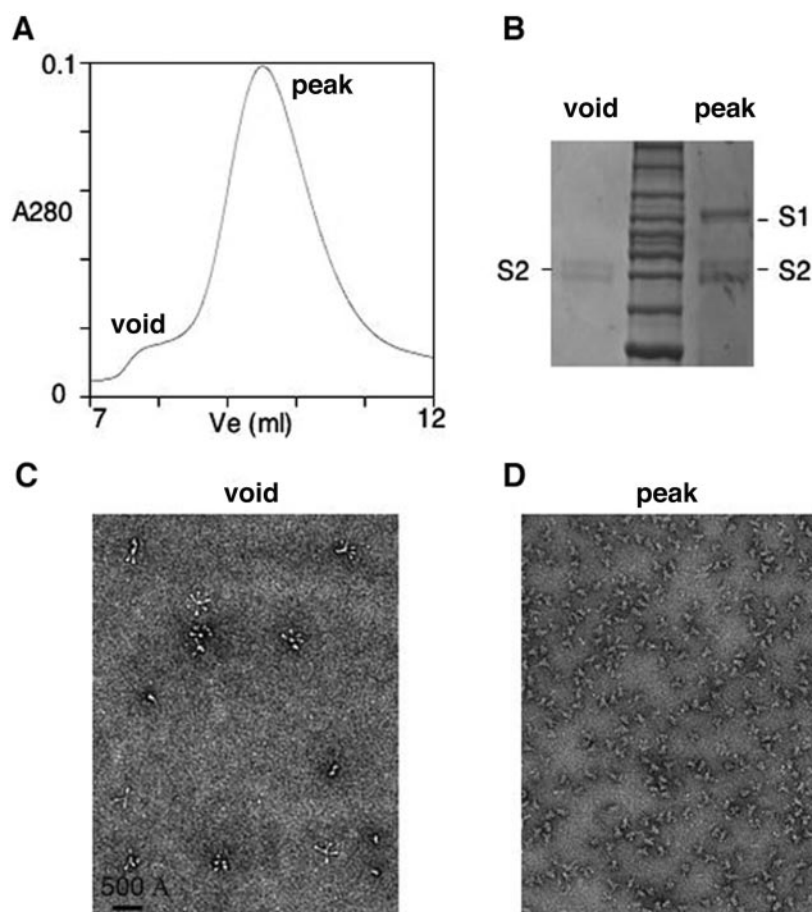


FIG. 5. Spontaneous rosette formation. (A) Chromatogram (A_{280}) of the S-e trimer digested with 200 ng/ml trypsin for 30 min at room temperature before quenching with PMSF and separation by gel filtration chromatography on Superdex 200. (B) Coomassie blue-stained reducing SDS-PAGE of protein from the void volume shows only S2, while the protein from the peak shows both S1 and S2. (C) Electron microscopy of a sample from the void volume of panel A, negatively stained with uranyl formate, showing undissociated, clove-shaped trimers. (D) Electron microscopy of a negatively stained sample from the peak of panel A, showing undissociated, clove-shaped trimers.

in vitro transition from monomer to trimer. Protease cleavage of the trimer does not alter its shape or structure, but the ensuing dissociation of S1 allows rearrangement of trimeric S2

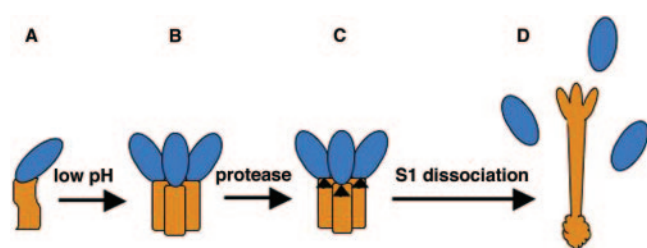


FIG. 6. States and transitions of S-e. (A) S-e monomer. S1, blue oval; S2, yellow rectangle, drawn here with curved lines to indicate flexibility. (B) S-e trimer. A low pH triggers trimerization and rigidification. (C) Cleaved S-e trimer. The arrows indicate the trypsin cleavage site at the junction of S1 and S2. (D) Rearranged S2 trimer. Dissociation of S1 occurs spontaneously, and it can be accelerated by exposure to 1 M urea. In this diagram, we depict the clustered fusion peptides of the three subunits as an irregularly outlined region at one end of the rearranged S2 shaft and the regions between HR1 and HR2 of the subunits as three ovals at the other end.

and formation of rosettes. Rosette formation is strictly dependent on the sequence of these transitions.

The flexible, secreted S-e monomer is a stable, folded molecule selectively sensitive to low concentrations of trypsin at the position corresponding to the known S1-S2 boundary in MHV. The S-e monomer is elongated and probably flexible in solution, as it yields a variety of images when contrasted in negative stain. The relatively common L-shaped images may reveal a hinge or kink between an S1 end and an S2 end. Consistent with this possibility, trypsin cleavage of monomeric S-e leads to rapid and complete dissociation of S1 from S2.

Exposure of intact S-e monomers to a pH between 5 and 6 (we have not determined a precise threshold) triggers irreversible trimerization, although a low pH does not appear to be required for trimerization of membrane-anchored S on virions (24). The clove-shaped trimers yield uniform images by negative-stain electron microscopy, indicating that trimerization rigidifies S-e. Monomers and trimers have similar contour lengths. Each of the three knobs at one end of a trimer probably corresponds to an S1 region, or some part of it, as it contains the RBD, and the stalk probably corresponds to trimer-clustered S2, perhaps with contributions from parts of S1.

Like S-e monomers, S-e trimers are specifically cleaved by low concentrations of trypsin between their S1 and S2 regions, but the fragments of the cleaved trimer dissociate much more slowly than those of the cleaved monomer. S1 dissociates from either monomeric or trimeric cleaved S-e as a soluble monomer with the same properties, but the S2 from which it separates has very different behavior. S2 from cleaved trimers is soluble, resists degradation by high concentrations of trypsin, and spontaneously rearranges into 250-Å-long, dumbbell-shaped rods that cluster at one end into rosettes. S2 from cleaved monomers aggregates and degrades upon exposure to high concentrations of protease. The properties of dissociated S1 and S2 suggest participation of S2, but not S1, in the tight contacts that mediate S-e trimerization.

The rearrangement and clustering of S2 resemble rosette formation by the influenza virus hemagglutinin (HA) fusogenic fragment (HA₂) after exposure to low pH and proteolytic degradation of the receptor-binding fragment (HA₁) (22). Clustering of hydrophobic fusion peptides at one end of rearranged HA₂ trimers produces the rosettes. We propose that the same is true for the elongated, rearranged S2 trimers that form after the dissociation of S1. When peptides corresponding to HR1 (96 residues) and HR2 (39 residues) of MHV S2 are mixed together, they assemble into stable, 145-Å-long rod-like structures, as expected for 96-residue α -helical coiled coils (2). Moreover, crystal structures of shorter fragments of MHV and SARS CoV S2 reveal a central three-chain coiled coil of HR1 peptides surrounded by three antiparallel segments of HR2 peptides (30, 31). Thus, coronavirus S2, like other class I fusion proteins, contains a trimer of hairpins in its postfusion conformation. The length of the central rod in the dumbbell-shaped subunit of SARS coronavirus S2 rosettes (Fig. 2D) is about 150 Å, consistent with the length of the coiled-coil element. The globular region at the distal end may represent a trimer of folded structures formed by the ~170 residues between HR1 and HR2. Our electron micrographs do not reveal details of the substructures at the center of the rosettes, but they are likely to contain the hydrophobic fusion peptide.

How do the states of the soluble ectodomain, described here, relate to events during entry of the SARS coronavirus into cells? In the envelope of mature virions (authentic or pseudotyped), the SARS CoV S protein is intact (18, 19). But trypsin treatment enhances fusion at neutral pH between Vero E6 and 293T cells expressing SARS CoV S protein (20, 21), and trypsin, thermolysin, or elastase treatment of cell-bound pseudovirions overcomes inhibition by lysosomotropic agents such as ammonium chloride and enhances infectivity (17, 20). Moreover, inhibitors of cathepsin L block SARS CoV infection (20). Thus, a critical functional cleavage appears to occur in the endosome, and we propose that trypsin might carry out the same step at the cell surface after virions bind ACE2. Ebola virus infectivity also requires endosomal cathepsins (4). We suggest that the transitions from S-e trimer (Fig. 2B) to cleaved trimer (Fig. 2C) to rearranged S2 (Fig. 2D) correspond to the familiar conformational changes that class I viral fusion proteins undergo as they mediate viral entry. The S2 rosettes have all of the characteristics of the final, postfusion conformation, especially in view of the lengths of coronavirus S2 HR1/HR2 complexes by electron microscopy (2). As cleavage and S1 dissociation are necessary for this *in vitro* rearrangement, we

propose that equivalent events occur during viral entry. The stability of the cleaved S-e trimer is not affected by a lowered pH (Fig. 5B), suggesting that proton binding does not help trigger dissociation of S1.

The S proteins of all coronaviruses have extensive similarity, especially in their S2 regions, but there is clearly considerable diversity in the details of entry mechanisms. The receptor-binding specificities vary; the conformational consequences of receptor binding differ; and the timing of proteolytic cleavage relative to virus release, attachment, and internalization differs. For example, the MHV S protein is cleaved into S1 and S2 by furin during its transport through the trans-Golgi network (5). It contacts the viral receptor, CEACAM1 (6, 26), through a domain in S1 that lies N terminal to the one homologous to the SARS CoV RBD (12). Receptor binding or exposure to pH 8 induces a conformational change in the MHV S2 domain, even if the furin cleavage site is removed (32). Our data suggest that cleavage of the SARS CoV S protein—probably at the S1-S2 boundary—is necessary to achieve an extended conformation in S2. This difference is consistent with the reliance by SARS CoV, but not by MHV, on endosomal cathepsins to enter cells (9, 20).

What is the significance of the SARS CoV S-e monomer and of its low-pH-induced transition to trimer? The role of a low pH in triggering trimerization of S-e *in vitro* is clearly distinct from the requirement that the virus pass through an acidified compartment during cell entry in order to facilitate cathepsin activity and cleavage (20). Moreover, SARS CoV S appears already to be a trimer on virions (24), and trimeric S-e in our micrographs resembles and the spikes seen in images of negatively stained coronavirus particles. Soluble ectodomains of other trimeric viral S proteins are often monomeric. For example, secreted recombinant influenza virus HA ectodomain and secreted human immunodeficiency virus gp140 (the ectodomain of gp160) are generally monomers (7), whereas membrane-anchored HA and gp160 are stable trimers, before and after cleavage. Thus, trimerization upon exposure to a low pH may simply be a useful biochemical property of secreted S-e. It may, however, be an indirect reflection of a functional conformational transition. For example, observations that trypsin cleavage enhances fusion and viral entry only after receptor binding (21) imply a role for a receptor-induced conformational change in S. Specific tryptic cleavage of the low-pH-induced S-e trimers at the S1-S2 boundary suggests that these trimers resemble receptor-bound spikes, at least in the way that they present themselves to trypsin. The monomer-trimer transition of S-e *in vitro* may therefore have some characteristics of the presumptive ACE2-induced conformational transition during viral infection *in vivo*.

ACKNOWLEDGMENTS

We thank Bing Chen, Yorgo Modis, and Susanne Swalley for discussions and technical help and David King and Arnie Falick at the Howard Hughes Medical Institute Mass Spectrometry Laboratory of the University of California (Berkeley) and Michael Berne at the Tufts Protein Chemistry Facility for mass spectrometry.

The molecular electron microscopy facility at Harvard Medical School is maintained by funds from National Institutes of Health grant P01-GM62580 (to David Derosier). This work was supported by National Institutes of Health grant CA13202 to S.C.H., who is an investigator in the Howard Hughes Medical Institute.

REFERENCES

1. Babcock, G. J., D. J. Eshshaki, W. D. Thomas, Jr., and D. M. Ambrosino. 2004. Amino acids 270 to 510 of the severe acute respiratory syndrome coronavirus spike protein are required for interaction with receptor. *J. Virol.* **78**:4552–4560.
2. Bosch, B. J., R. van der Zee, C. A. de Haan, and P. J. Rottier. 2003. The coronavirus spike protein is a class I virus fusion protein: structural and functional characterization of the fusion core complex. *J. Virol.* **77**:8801–8811.
3. Cavanagh, D. 1995. The coronavirus surface glycoprotein. Plenum Press, New York, N.Y.
4. Chandran, K., N. J. Sullivan, U. Felbor, S. P. Whelan, and J. M. Cunningham. 2005. Endosomal proteolysis of the Ebola virus glycoprotein is necessary for infection. *Science* **308**:1643–1645.
5. de Haan, C. A., K. Stadler, G. J. Godeke, B. J. Bosch, and P. J. Rottier. 2004. Cleavage inhibition of the murine coronavirus spike protein by a furin-like enzyme affects cell-cell but not virus-cell fusion. *J. Virol.* **78**:6048–6054.
6. Dveksler, G. S., M. N. Pensiero, C. B. Cardellicchio, R. K. Williams, G. S. Jiang, K. V. Holmes, and C. W. Dieffenbach. 1991. Cloning of the mouse hepatitis virus (MHV) receptor: expression in human and hamster cell lines confers susceptibility to MHV. *J. Virol.* **65**:6881–6891.
7. Earl, P. L., R. W. Doms, and B. Moss. 1990. Oligomeric structure of the human immunodeficiency virus type 1 envelope glycoprotein. *Proc. Natl. Acad. Sci. USA* **87**:648–652.
8. Eckert, D. M., and P. S. Kim. 2001. Mechanisms of viral membrane fusion and its inhibition. *Annu. Rev. Biochem.* **70**:777–810.
9. Huang, I.-C., B. J. Bosch, F. Li, W. Li, K. H. Lee, S. Ghiran, N. Vasileva, T. S. Dermody, S. C. Harrison, P. R. Dormitzer, M. Farzan, P. J. Rottier, and H. Choe. 2006. SARS coronavirus, but not human coronavirus NL63, utilizes cathepsin L to infect ACE2-expressing cells. *J. Biol. Chem.* **281**:3198–3203.
10. Klenk, H. D., and W. Garten. 1994. Host cell proteases controlling virus pathogenicity. *Trends Microbiol.* **2**:39–43.
11. Ksiazek, T. G., D. Erdman, C. S. Goldsmith, S. R. Zaki, T. Peret, S. Emery, S. Tong, C. Urbani, J. A. Comer, W. Lim, P. E. Rollin, S. F. Dowell, A. E. Ling, C. D. Humphrey, W. J. Shieh, J. Guarner, C. D. Paddock, P. Rota, B. Fields, J. DeRisi, J. Y. Yang, N. Cox, J. M. Hughes, J. W. LeDuc, W. J. Bellini, and L. J. Anderson. 2003. A novel coronavirus associated with severe acute respiratory syndrome. *N. Engl. J. Med.* **348**:1953–1966.
12. Kubo, H., Y. K. Yamada, and F. Taguchi. 1994. Localization of neutralizing epitopes and the receptor-binding site within the amino-terminal 330 amino acids of the murine coronavirus spike protein. *J. Virol.* **68**:5403–5410.
13. Lai, M. M. C., and K. V. Holmes. 2001. Coronaviridae: the viruses and their replication, p. 1163–1186. *In* D. M. Knipe and P. M. Howley (ed.), *Fields virology*, fourth ed. Lippincott Williams & Wilkins, Philadelphia, Pa.
14. Li, F., W. Li, M. Farzan, and S. C. Harrison. 2005. Structure of SARS coronavirus spike receptor-binding domain complexed with receptor. *Science* **309**:1864–1868.
15. Li, W., M. J. Moore, N. Vasileva, J. Sui, S. K. Wong, M. A. Berne, M. Somasundaran, J. L. Sullivan, K. Luzuriaga, T. C. Greenough, H. Choe, and M. Farzan. 2003. Angiotensin-converting enzyme 2 is a functional receptor for the SARS coronavirus. *Nature* **426**:450–454.
16. Marra, M. A., S. J. Jones, C. R. Astell, R. A. Holt, A. Brooks-Wilson, Y. S. Butterfield, J. Khattra, J. K. Asano, S. A. Barber, S. Y. Chan, A. Cloutier, S. M. Coughlin, D. Freeman, N. Girn, O. L. Griffith, S. R. Leach, M. Mayo, H. McDonald, S. B. Montgomery, P. K. Pandoh, A. S. Petrescu, A. G. Robertson, J. E. Schein, A. Siddiqui, D. E. Smailus, J. M. Stott, G. S. Yang, F. Plummer, A. Andonov, H. Artsob, N. Bastien, K. Bernard, T. F. Booth, D. Bowness, M. Czub, M. Drebot, L. Fernando, R. Flick, M. Garbutt, M. Gray, A. Grolla, S. Jones, H. Feldmann, A. Meyers, A. Kabani, Y. Li, S. Normand, U. Stroher, G. A. Tipples, S. Tyler, R. Vogrig, D. Ward, B. Watson, R. C. Brunham, M. Krajden, M. Petric, D. M. Skowronski, C. Upton, and R. L. Roper. 2003. The genome sequence of the SARS-associated coronavirus. *Science* **300**:1399–1404.
17. Matsuyama, S., M. Ujike, S. Morikawa, M. Tashiro, and F. Taguchi. 2005. Protease-mediated enhancement of severe acute respiratory syndrome coronavirus infection. *Proc. Natl. Acad. Sci. USA* **102**:12543–12547.
18. Peiris, J. S., S. T. Lai, L. L. Poon, Y. Guan, L. Y. Yam, W. Lim, J. Nicholls, W. K. Yee, W. W. Yan, M. T. Cheung, V. C. Cheng, K. H. Chan, D. N. Tsang, R. W. Yung, T. K. Ng, and K. Y. Yuen. 2003. Coronavirus as a possible cause of severe acute respiratory syndrome. *Lancet* **361**:1319–1325.
19. Rota, P. A., M. S. Oberste, S. S. Monroe, W. A. Nix, R. Campagnoli, J. P. Icenogle, S. Penaranda, B. Bankamp, K. Maher, M. H. Chen, S. Tong, A. Tamin, L. Lowe, M. Frace, J. L. DeRisi, Q. Chen, D. Wang, D. D. Erdman, T. C. Peret, C. Burns, T. G. Ksiazek, P. E. Rollin, A. Sanchez, S. Liffick, B. Holloway, J. Limor, K. McCaustland, M. Olsen-Rasmussen, R. Fouchier, S. Gunther, A. D. Osterhaus, C. Drosten, M. A. Pallansch, L. J. Anderson, and W. J. Bellini. 2003. Characterization of a novel coronavirus associated with severe acute respiratory syndrome. *Science* **300**:1394–1399.
20. Simmons, G., D. N. Gosalia, A. J. Rennekamp, J. D. Reeves, S. L. Diamond, and P. Bates. 2005. Inhibitors of cathepsin L prevent severe acute respiratory syndrome coronavirus entry. *Proc. Natl. Acad. Sci. USA* **102**:11876–11881.
21. Simmons, G., J. D. Reeves, A. J. Rennekamp, S. M. Amberg, A. J. Piefer, and P. Bates. 2004. Characterization of severe acute respiratory syndrome-associated coronavirus (SARS CoV) spike glycoprotein-mediated viral entry. *Proc. Natl. Acad. Sci. USA* **101**:4240–4245.
22. Skehel, J. J., P. M. Bayley, E. B. Brown, S. R. Martin, M. D. Waterfield, J. M. White, I. A. Wilson, and D. C. Wiley. 1982. Changes in the conformation of influenza virus hemagglutinin at the pH optimum of virus-mediated membrane fusion. *Proc. Natl. Acad. Sci. USA* **79**:968–972.
23. Skehel, J. J., and D. C. Wiley. 2000. Receptor binding and membrane fusion in virus entry: the influenza hemagglutinin. *Annu. Rev. Biochem.* **69**:531–569.
24. Song, H. C., M. Y. Seo, K. Stadler, B. J. Yoo, Q. L. Choo, S. R. Coates, Y. Uematsu, T. Harada, C. E. Greer, J. M. Polo, P. Pileri, M. Eickmann, R. Rappuoli, S. Abrignani, M. Houghton, and J. H. Han. 2004. Synthesis and characterization of a native, oligomeric form of recombinant severe acute respiratory syndrome coronavirus spike glycoprotein. *J. Virol.* **78**:10328–10335.
25. Spaan, W., D. Cavanagh, and M. C. Horzinek. 1988. Coronaviruses: structure and genome expression. *J. Gen. Virol.* **69**(Pt. 12):2939–2952.
26. Williams, R. K., G. S. Jiang, and K. V. Holmes. 1991. Receptor for mouse hepatitis virus is a member of the carcinoembryonic antigen family of glycoproteins. *Proc. Natl. Acad. Sci. USA* **88**:5533–5536.
27. Wilson, I. A., J. J. Skehel, and D. C. Wiley. 1981. Structure of the haemagglutinin membrane glycoprotein of influenza virus at 3 Å resolution. *Nature* **289**:366–373.
28. Wong, S. K., W. Li, M. J. Moore, H. Choe, and M. Farzan. 2004. A 193-amino acid fragment of the SARS coronavirus S protein efficiently binds angiotensin-converting enzyme 2. *J. Biol. Chem.* **279**:3197–3201.
29. Xiao, X., S. Chakraborti, A. S. Dimitrov, K. Gramatikoff, and D. S. Dimitrov. 2003. The SARS CoV S glycoprotein: expression and functional characterization. *Biochem. Biophys. Res. Commun.* **312**:1159–1164.
30. Xu, Y., Y. Liu, Z. Lou, L. Qin, X. Li, Z. Bai, H. Pang, P. Tien, G. F. Gao, and Z. Rao. 2004. Structural basis for coronavirus-mediated membrane fusion. Crystal structure of mouse hepatitis virus spike protein fusion core. *J. Biol. Chem.* **279**:30514–30522.
31. Xu, Y., Z. Lou, Y. Liu, H. Pang, P. Tien, G. F. Gao, and Z. Rao. 2004. Crystal structure of severe acute respiratory syndrome coronavirus spike protein fusion core. *J. Biol. Chem.* **279**:49414–49419.
32. Zelus, B. D., J. H. Schickli, D. M. Blau, S. R. Weiss, and K. V. Holmes. 2003. Conformational changes in the spike glycoprotein of murine coronavirus are induced at 37°C either by soluble murine CEACAM1 receptors or by pH 8. *J. Virol.* **77**:830–840.